Using nanopillars of silicon oxide as a versatile platform for visualizing a selective immunosorbent

Jem-Kun Chen, Gang-Yan Zhou, Chih-Feng Huang, and Fu-Hsiang Ko

---

Articles you may be interested in
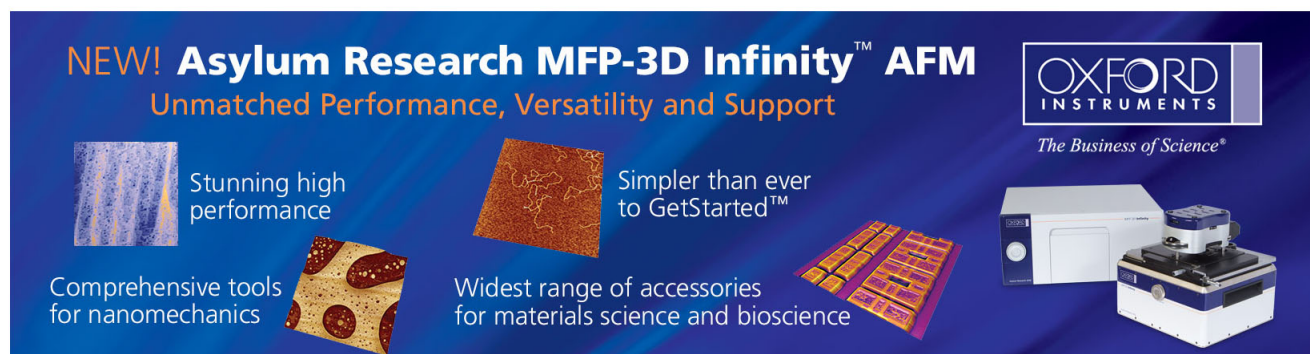
Label-free electronic probing of nucleic acids and proteins at the nanoscale using the nanoneedle biosensor
Biomicrofluidics **7**, 044114 (2013); 10.1063/1.4817771

Ultrasensitive food toxin biosensor using frequency based signals of silicon oxide nanoporous structure
Appl. Phys. Lett. **102**, 243701 (2013); 10.1063/1.4811409

Nano-islands integrated evanescence-based lab-on-a-chip on silica-on-silicon and polydimethylsiloxane hybrid platform for detection of recombinant growth hormone
Biomicrofluidics **6**, 046501 (2012); 10.1063/1.4757968

Sensing properties of infrared nanostructured plasmonic crystals fabricated by electron beam lithography and argon ion milling
J. Vac. Sci. Technol. B **30**, 06FE02 (2012); 10.1116/1.4767274

Nanostructured nickel oxide film for application to fish freshness biosensor
Appl. Phys. Lett. **101**, 023703 (2012); 10.1063/1.4736578

Using nanopillars of silicon oxide as a versatile platform for visualizing a selective immunosorbent

Jem-Kun Chen,[1,a)] Gang-Yan Zhou,[1] Chih-Feng Huang,[2] and Fu-Hsiang Ko[3]

[1]*Department of Materials Science and Engineering, National Taiwan University of Science and Technology, 43, Sec. 4, Keelung Road, Taipei 106, Taiwan*

[2]*Department of Chemical Engineering, National Chung Hsing University, Eng. Bld. 3, 250 Kuo Kuang Road, 402 Taichung, Taiwan*

[3]*Department of Applied Chemistry, Materials and Science Engineering, National Chiao Tung University, 1001, University Road, Hsinchu 300, Taiwan*

In this study, we fabricated nanopillar arrays of silicon oxide for use as two-dimensional periodic relief gratings (2DPRGs) on Si surfaces. We deposited antibodies onto the pillar surfaces of 2DPRGs modified with protein G to obtain optical detectors that were specific for the targeted antigen; the antigen units that filled the spaces between the nanopillars of the 2DPRG lead to a dramatic change in the pillar scale. The effective refractive index (n_{eff}) of the 2DPRGs was related to the pillar scale of the 2DPRG; after coupling of the antigen, a color change from pure green to orange was observable. © *2013 AIP Publishing LLC*. [http://dx.doi.org/10.1063/1.4812340]

Several optical biological sensors that function based on the measurement of diffraction patterns as assay readouts have been reported recently. In addition, optical-label-free detection methods can also be employed, including surface plasmon resonance (SPR) spectroscopy,[1] Mach–Zehnder interferometry (MZI),[2] fiber optic techniques,[3] and waveguides.[4] Optical reflectometry, SPR spectroscopy, and ellipsometry are all based on the detection of changes in refractive index; although they can provide useful estimates of the degree of adsorption on a surface, they are inherently insensitive to the layer thickness and composition.[5,6] The detection of proteins in a sensitive and rapid manner is essential in a variety of clinical applications; accordingly, many antibody-based immunoassay systems have been developed as recognition elements for detecting proteins.[7] In addition, biosensors based on optical diffraction have also been demonstrated for recognizing the binding events of various biomolecules; they operate based on changes in effective height or refractive index on periodically patterned gratings.[8] The antibodies that have been used as recognition elements in most biosensing platforms are generally those produced *in vivo*.[9] Although antibodies are unique in their ability to transduce the recognition of antigens into readily observable signals, small quantities of antigens can be difficult to detect using antibodies alone, pointing to a need for signal enhancement schemes.

Subwavelength structured (SWS) surfaces are attractive materials for many different optical elements. Through careful design of an SWS surface, highly efficient diffraction gratings can be synthesized, even with a binary profile. When the SWS element is a one-dimensional (1-D) or an unsymmetrical two-dimensional (2-D) periodic surface, the effective refractive index depends upon the polarization state of the incident light.[10,11] Nanopillar (NPL) arrays are SWS surfaces—symmetrical 2-D periodic surfaces—that are currently attracting great interest for their potential applications in grating or photonics.[12] NPLs have unique optical properties that result from their 1-D geometries, including polarized photoresponses, diameter-tunable band structures, and biosensing ability.[13,14] When the NPLs interact specifically or nonspecifically with target molecules, changes typically occur to the geometrical parameters of the gratings and/or the refractive index contrast.[15]

In many studies, the detection of small amounts of biomolecules has required additional signal enhancement,[16] either through microfabrication of solid diffraction gratings or through the use of *in situ*–assembled diffraction gratings self-fabricated from nano- or micro-sized particles. In this study, we employed NPL arrays of silica oxide—generated using lithography and reactive ion etching (RIE)—as two-dimensional periodic relief gratings (2DPRGs) to increase the dimensions of the interface available for protein adsorption and, thereby, enhance the optical sensitivity. Sequentially, we immobilized antibodies on the surfaces of the NPL arrays and used them to couple with antigens from sample solutions, thereby changing the geometrical parameters (filling factor) and the refractive indices of the gratings (Figure 1). Detection of the bound antigens was possible by illuminating the surface with visible light that diffracted after the binding of the biological material. This versatile process appears to be amenable to the creation of large-area uniform coatings on essentially any surface with precise control over the scale of the silicon oxide pillars and the optical properties of the antibodies.

Figure 2 outlines the basic strategy for the fabrication of an antibody-modified NPL array using the very-large-scale integration (VLSI) process and RIE. (A) First, deposition was performed through plasma-enhanced chemical vapor deposition. A silicon oxide film was deposited on the wafer, with the oxygen atoms supplied by tetraethoxysilane (TEOS).[17] The Si wafer was then treated with hexamethyldisilazane (HMDS) to transform the OH groups on the surface of wafer into an inert film of $SiMe_3$ groups.[18] (B) Next, a negative

a)Author to whom correspondence should be addressed. Electronic mail: jkchen@mail.ntust.edu.tw. Tel.: +886-2-27376523. Fax: +886-2-27376544.
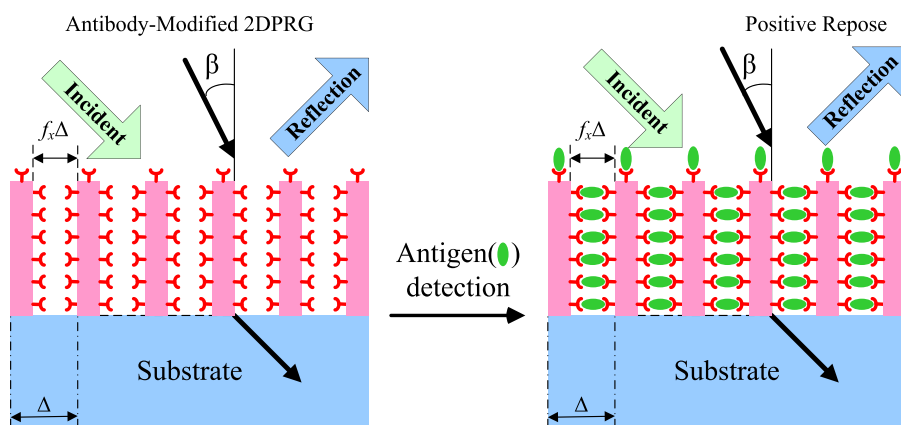
FIG. 1. Schematic representation of the cross-section of the sensor—a symmetric 2-D periodic relief grating (2DPRG) with FF in the x direction (f_x). The geometrical parameters changed when antigens attached to the antibody-modified 2DPRG; they could be detected through ellipsometry when illuminating the 2DPRG.

photoresist was spun on the HMDS-treated Si wafer. Advanced lithography was then employed to pattern the photoresist with a NPL array of 300 nm scale after development. (C) RIE was used for dry etching after the photoresist had
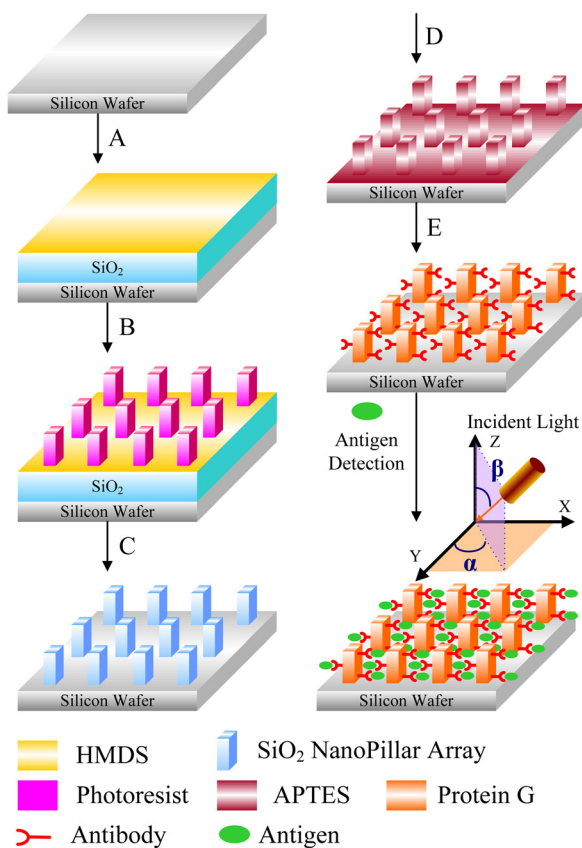

FIG. 2. Schematic representation of the process used to fabricate the MAHA-modified 2DPRG. (A) Silicon oxide film deposited using plasma-enhanced chemical vapor deposition; the surface was treated with HMDS in a thermal evaporator. (B) Negative photoresist was spun on the HMDS-treated surface to pattern the photoresist as a 300-nm-scale NPL array. (C) Only the exposed regions of silicon dioxide were dry-etched by supplying a mixture of CHF_3 and CF_4 gases; sequentially, the remaining photoresist hard mask was removed from the surface by solvents. (D) The 2DPRG of silicon oxide was treated with ATPES to present amino groups from the surface. (E) ProG was activated in a solution of EDC and NHS for reaction with the amino groups on the surface of the 2DPRG and, thereby, immobilization on the pillar surface; MAHA units were oriented on the proG-modified pillar surface; the presence of MHHA could be detected using ellipsometry; schematic representation of light traveling through a 2DPRG surface with incident angles α and β.

been patterned onto the surface to cover the silicon oxide as a protection mask. The remaining photoresist hard mask was removed from the surface through the action of solvents, leaving behind a 2DPRG (NPL array) of silicon oxide. (D) The 2DPRG of silicon oxide was immersed in a solution of 3-aminopropyltriethoxysilane in toluene, resulting in a surface presenting amino groups.[19] (E) Commercially available recombinant protein G (proG), which minimizes nonspecific interactions of serum/cell proteins, was covalently immobilized on the NPL surface through conjugation to the amino groups to give a proG-2DPRG. The presence of ProG ensured efficient orientation of the antibody units. The proG was activated through the addition of N-ethyl-N'-(3-dimethylaminopropyl)carbodiimide hydrochloride (EDC) and N-hydroxysuccinimide (NHS) before reacting with the amino groups on the pillar surface of the 2DPRG. Antibodies were then deposited on the NPL surface through interactions with the immobilized proG, thereby yielding a promising general platform for the specific and sensitive detection of antigens through a mechanism involving changes in effective refractive index.[20] In particular, purified mouse anti-human albumin was successively immobilized with efficient orientation on the surface of the proG-2DPRG conjugates. The MAHA-modified 2DPRGs were then incubated overnight with the target [purified mouse HRP-human albumin (MHHA)] and the control [bovine serum albumin (BSA)] at various concentrations in phosphate-buffered saline (PBS). Ellipsometry and atomic force microscopy (AFM) were used to determine the effective refractive indices and morphologies, respectively, of the 2DPRGs after selective deposition of the immunosorbent and lyophilization to preserve the structure formed in aqueous solutions.

To obtain useful artificial dielectric elements, it must be possible to relate the effective refractive index to the grating profile in a simple way. By solving Maxwell's equations with relevant boundary conditions, many authors have obtained the effective refractive indices of 1-D and 2-D subwavelength gratings.[21] Alternatively, effective medium theory generally yields a good approximation if the period-to-wavelength ratio is sufficiently small. For 1-D gratings, the theory gives the following simple expressions for the ordinary and extraordinary indices:

$$n_{TE}{}^2 = f_1 n_1{}^2 + f_2 n_2{}^2, \tag{1}$$

$$n_{TM}{}^{-2} = f_1 n_1{}^{-2} + f_2 n_2{}^{-2}, \tag{2}$$

where f_1 is the fill factor (FF) for medium 1 and f_2 (equal to $1-f_1$) is the FF for medium 2. The refractive index in the direction normal to the grating vectors of a 2-D subwavelength grating is given in effective-medium theory by

$$n_{eff} = [(1 - f_x f_y)n_1{}^2 + f_x f_y n_2{}^2]^{1/2}, \tag{3}$$

where f_x and f_y are the FFs of medium 2 in the x and y directions, respectively (Figure 1). It has been noted that there are no simple closed-form zero-order expressions for the transverse principal effective indices of a 2-D subwavelength grating; on the other hand, the indices can be bounded approximately by using the simple expressions derived from effective medium theory.[22] For simplicity, we will consider rectangular cylindrical geometries only. To set the upper bound, we view the 2-D rectangular grating as a 1-D grating consisting of strips aligned perpendicular to the electric field. Each strip in turn can be considered as a section of a 1-D grating with ridges parallel to the electric field. We used Eq. (1) to calculate the effective index of each strip; we then combined these strip indices with Eq. (2) to calculate the overall effective refractive index. This effective refractive index is an upper bound that is exact in the static case; it is given by

$$n_{eff,upper} = \left[\frac{1 - f_x}{n_1{}^2} + \frac{f_x}{f_y n_2{}^2 + (1 - f_y)n_1{}^2} \right]^{-1/2}. \tag{4}$$

To obtain the lower bound, we considered the 2-D grating to be a 1-D grating consisting of strips parallel to the electric field. We could now use Eq. (2) to determine the effective refractive index of each strip and Eq. (1) to determine the overall effective refractive index, representing the lower bound, giving

$$n_{eff,lower} = \left[(1 - f_y)n_1{}^2 + \frac{f_y}{f_x n_2{}^{-2} + (1 - f_x)n_1{}^{-2}} \right]^{1/2}. \tag{5}$$

We obtained the bounds of the effective refractive index in the y direction by interchanging the x and y subscripts. At all times, the bounds lay between the indices of the two components of the artificial dielectric.

When the antibody-modified 2DPRGs coupled specifically with the target antigen, we typically observed changes in the geometrical parameters of the 2DPRGs and/or the refractive index contrast. According to the effective-medium theory, the FFs in the x (f_x) and y (f_y) directions represent the pillar scales. We used AFM to visualize the morphologies of the antibody-modified 2DPRGs. The three-dimensional (3-D), 2-D, and line cross-section analysis AFM topographic images of the lyophilized MAHA-modified 2DPRG reveal (Figure 3(a)) that the MAHA-modified 2DPRG on the Si surface existed as a dense distinctive overlayer, with an average pillar width of approximately 316 nm and space of 865 nm, within a scanning area of $5 \times 5 \, \mu m$. The texture of the pillar array was clearly evident in the line cross-section analysis. Each pillar of the antibody-modified 2DPRG was positioned in a regular array with a height of 469 ± 3 nm. The 2DPRG comprised a repeating pattern of pillars and spaces over a large area. The MAHA units bound to the pillar surface

retained their ability to recognize and bind their antigen efficiently and specifically.[23] Figure 3(b) displays 3-D, 2-D, and line cross-section analysis AFM topographic images of the lyophilized antibody-modified 2DPRG after coupling to the target antigen. The regular pillar array remained after the binding of the target antigen, with the scale of each pillar increasing from 316 ± 3 to 584 ± 3 nm, resulting in a decreased distance between the pillars; we calculated the thickness of the target antigen layer to be approximately 134 nm the aqueous solution. To magnify the changes in the geometrical parameters of the antibody-modified 2DPRG after antigen coupling, we selected MAHA because it is relatively large compared with more-typical target analytes. Note that small molecules, such as haptens, aflatoxins, ochratoxins, etc., may not be detected by this method with sufficient sensitivity. To verify that the MHHA units were bound only to the MAHA-modified areas, we also tested the binding of BSA to the surface. We observed no apparent variation in the geometrical parameters over the entire sample area in the presence of BSA, confirming the functionality and specificity of the antigens after capture by the protG-2DPRG.

When measured at 632.8 nm using ellipsometry, we obtained a standard value for the refractive index of the MHHA thin film of 1.4374, close to those values reported previously.[24] Figure 4(a) displays the values of n_{eff} of the bare 2DPRG (A), proG-2DPRG (B), and antibody-proG-2DPRG (C) as measured at a wavelength of 633 nm. The refractive index of MHHA was close to that of silicon oxide (1.46); therefore, we regarded it as the same component in effective medium theory. A dramatic response in the value of n_{eff} occurred specifically after MHHA had coupled with MAHA on the pillar surface, as probed using ellipsometry (Figure 4(a), D). In addition, the value of n_{eff} of the MAHA-modified 2DPRG was relatively unchanged after its immersion in the control solution of BSA, suggesting that the BSA units did not couple significantly with the MAHA film on the pillar surface (Figure 4(a), E). Photographic images of the MAHA-modified 2DPRG before and after antigen coupling, obtained at an angle β of approximately 10°–20° (Figure 1), are presented in the insets to Figure 4(a). We formed the 2DPRG into a die using an etching process and a 1 cm $\times$ 1 cm contact mask. In this study, we observed the reflection of the 2DPRG by the naked eye under an invariable angle β.[25] At an angle β in the range 15°, the antibody-modified 2DPRG displayed a pure green color prior to coupling with MHHA; after coupling, the color underwent an obvious change to orange. Such visualized color changes appear to have potential applicability in the rapid and convenient detection of specific antigens. Because the effect of a diffractive grating is dependent on the period and/or the angle of observation when the structural scale of the grating is greater than the wavelength, for this study we employed fixed values of the period and angle of observation. Furthermore, we considered the air layer of the 2DPRG to be filled with silicon oxide and the antigen; in Eq. (3), n_1 and n_2 represent the refractive indices of air and silicon oxide/antigen, respectively. To describe the square pillar structure, for convenience we set the FFs in the x directions (f_x) to be equal to those in the y direction (f_y). Equations (3)–(5) could, therefore, be rewritten as follows as Eqs. (6)–(8), respectively,
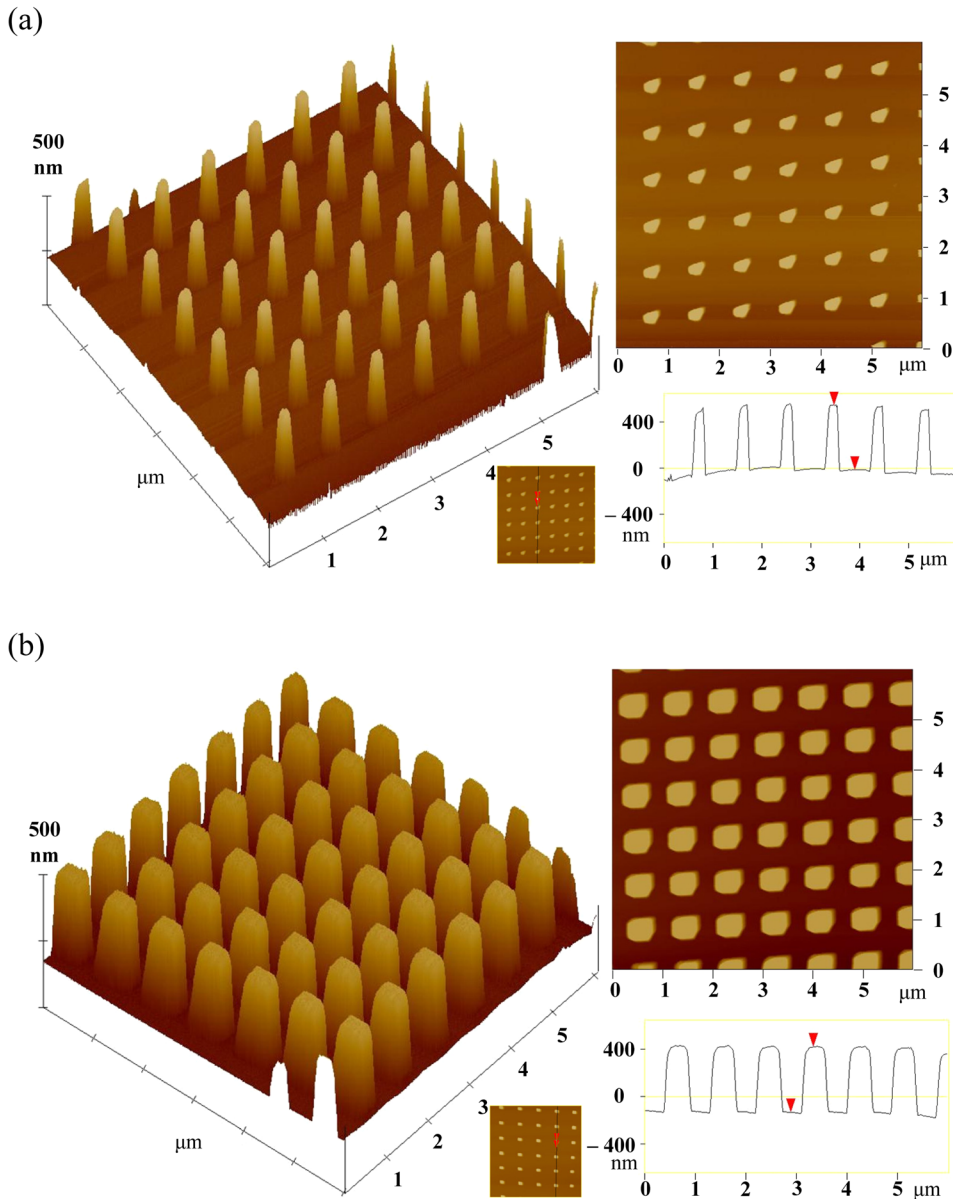
(a)

(b)

FIG. 3. 3-D (left), 2-D (upper right), and line cross-section analysis (lower right) AFM topographic images of the MAHA-modified 2DPRG (a) before and (b) after coupling with MHHA.

$$n_{eff} = [(1-f^2)n_1{}^2 + f^2 n_2{}^2]^{1/2}, \tag{6}$$

$$n_{eff,upper} = \left[\frac{1-f}{n_1{}^2} + \frac{f}{fn_2{}^2 + (1-f)n_1{}^2}\right]^{-1/2}, \tag{7}$$

$$n_{eff,lower} = \left[(1-f)n_1{}^2 + \frac{f}{fn_2{}^{-2} + (1-f)n_1{}^{-2}}\right]^{-1/2}. \tag{8}$$

We calculated the values of f from the measured values of n_{eff}, calculated from the change in pillar scale during the antigen coupling process. The effective medium theory is most accurate when the period is sufficiently smaller than the wavelength. Therefore, we use the expressions for the bounded indices to fit our results. It has been reported previously that the effective indices were, on average, increased by at most 3% for a 2-D 400-nm-period symmetric grating at a wavelength of 633 nm.[26] Therefore, we expected the inaccuracy of the refractive indices for the 300-nm-scale 2DPRG at a wavelength of 633 nm to be on the order of less than 3%.

Figure 4(a) also presents the dependence of the value of f of the 2DPRG, calculated using Eq. (6), on the value of n_{eff} for the 2DPRG (A), proG-2DPRG (B), antibody-proG-2DPRG (C), antibody-proG-2DPRG after antigen coupling (D), and antibody-proG-2DPRG after BSA absorption (E). Our data suggest that the MAHA-modified 2DPRG underwent an increase in the filling volume when the antigen surrounded the pillar structure. Moreover, we used the model equations (7) and (8) for the effective medium theory to evaluate these values of n_{eff} and f for these samples; we constructed these equations to fit the data only at 633 nm, thereby avoiding the lower wavelength regions that are strongly absorbed by the surface cover slip, as revealed in Figure 4(b). Upon increasing the concentration of MHHA, the values of n_{eff} fitted well within the bounded regions defined using Eqs. (7) and (8), even though we had assumed that the refractive indices of silicon oxide and MHHA were equal. The upward concavity in the values of n_{eff} of the 2-D pillar array as a function of the FFs is consistent with previous reports.[24,26] The model matched the measured data perfectly at various antigen
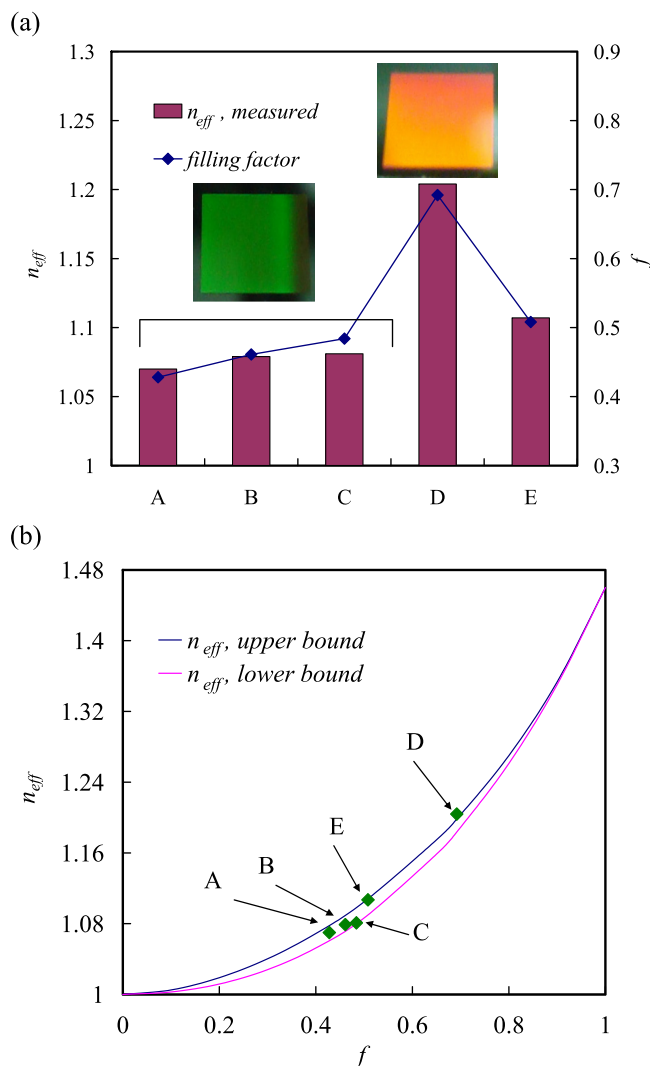
(a)

(b)

FIG. 4. (a) Values of n_{eff}, measured using ellipsometry, of (A) bare 2DPRG, (B) proG-2DPRG, (C) MAHA-modified 2DPRG, (D) MAHA-modified 2DPRG after coupling with MHHA, and (E) MAHA-modified 2DPRG after binding BSA (control). Photographic images for (A)–(C) and (D) demonstrate the grating effect of the 2DPRG. (b) Values of n_{eff} plotted with respect to the calculated values of f for (A)–(E) and fitted to Eqs. (7) and (8).

concentrations during the MHHA coupling process. Our findings indicate that the inherent sensitivity of the ellipsometric measurement of the change in refractive index across the interface as a result of protein adsorption was enhanced when using the 2DPRG structure.

We have substantially modified a specific antibody onto the pillared surface over a large area with the capability of antigen detection. By selecting a suitably functional antibody and optimizing the coupling process with the antigen, the scale of the nanostructures was readily altered. We suspect that this simple sensor might also exhibit an apparent color change for the detection of any cell featuring a specific antigen having sufficient volume to fill in the pillar structure when bound to a silicon surface.

[1]Q. Gan, Y. Gao, and F. J. Bartoli, Opt. Express **17**, 20747–20755 (2009).
[2]B. J. Luff, J. S. Wilkinson, J. Piehler, U. Hollenbach, J. Ingenhoff, and N. Fabricius, J. Lightwave Technol. **16**, 583–592 (1998).
[3]I. Del Villar, I. R. Matias, F. J. Arregui, and J. M. Corres, Opt. Eng. **45**, 104401 (2006).
[4]R. Yan, S. P. Mestas, G. Yuan, R. Safaisini, D. S. Dandy, and K. L. Lear, Lab Chip **9**, 2163–2168 (2009).
[5]H. Neubert, E. S. Jacoby, S. S. Bansal, R. K. Iles, D. A. Cowan, and A. T. Kicman, Anal. Chem. **74**, 3677–3683 (2002).
[6]W. Yeh, J. Kleingartner, and A. C. Hillier, Anal. Chem. **82**, 4988–4993 (2010).
[7]S. J. Kim, K. V. Gobi, H. Tanaka, Y. Shoyama, and N. Miura, Chem. Lett. **35**, 1132–1133 (2006).
[8]R. Jenison, S. Yang, A. Haeberli, and B. Polisky, Nat. Biotechnol. **19**, 62–65 (2001).
[9]W. Zhao, W.-P. Zhang, Z.-L. Zhang, R.-L. He, Y. Lin, M. Xie, H.-Z. Wang, and D.-W. Pang, Anal. Chem. **84**, 2358–2365 (2012).
[10]J. K. Chen and B. J. Bai, J. Phys. Chem. C **115**, 21341–21350 (2011).
[11]J.-K. Chen, P.-C. Pai, J.-Y. Chang, and S.-K. Fan, ACS Appl. Mater. Interfaces **4**, 1935–1947 (2012).
[12]Z. Szabó, J. Volk, E. Fülöp, A. Deák, and I. Bársony, Photonics Nanostruct. **11**, 1–7 (2013).
[13]M. Hirade, H. Nakanotani, M. Yahiro, and C. Adachi, ACS Appl. Mater. Interfaces **3**, 80–83 (2011).
[14]J.-K. Chen, J.-H. Wang, S.-K. Fan, and J.-Y. Chang, J. Phys. Chem. C **116**, 6980–6992 (2012).
[15]G. Ye and X. Wang, Biosens. Bioelectron. **26**, 772–777 (2010).
[16]C. L. Chang, G. Acharya, and C. A. Savran, Appl. Phys. Lett. **90**, 233901 (2007).
[17]Y. Dinga, Q. Pana, J. Jina, H. Jiab, and H. Shirai, Thin Solid Films **518**, 3487–3491 (2010).
[18]J. K. Chen and A.-L. Zhuang, J. Phys. Chem. C **114**, 11801–11809 (2010).
[19]J. K. Chen, C. Y. Hsieh, C. F. Huang, P. M. Li, S. W. Kuo, and F. C. Chang, Macromolecules **41**, 8729–8736 (2008).
[20]J. M. Lee, H. K. Park, Y. Jung, J. K. Kim, S. O. Jung, and B. H. Chung, Anal. Chem. **79**, 2680–2687 (2007).
[21]E. B. Grann, M. G. Moharam, and D. A. Pommet, J. Opt. Soc. Am. A **11**, 2695–2703 (1994).
[22]J. L. Jackson and S. R. Coriell, J. Appl. Phys. **39**, 2349 (1968).
[23]B. Akerström and L. Björck, J. Biol. Chem. **261**, 10240–10247 (1986).
[24]H. Kikuta, H. Toyota, and W. Yui, Opt. Rev. **10**, 63–73 (2003).
[25]Z. Burton and B. Bhushan, Nano Lett. **5**, 1607–1613 (2005).
[26]F. T. Chen and H. G. Craighead, Opt. Lett. **20**, 121–123 (1995).